CDDpress

www.nature.com/cddis

ARTICLE OPEN

Check for updates

miR-28-based combination therapy impairs aggressive B cell lymphoma growth by rewiring DNA replication

Teresa Fuertes[1], Emigdio Álvarez-Corrales[2], Carmen Gómez-Escolar[1], Patricia Ubieto-Capella[3], Álvaro Serrano-Navarro[1], Antonio de Molina[4], Juan Méndez[3], Almudena R. Ramiro[1,5]✉ and Virginia G. de Yébenes[2,5]✉

Diffuse large B cell lymphoma (DLBCL) is the most common aggressive B cell lymphoma and accounts for nearly 40% of cases of B cell non-Hodgkin lymphoma. DLBCL is generally treated with R-CHOP chemotherapy, but many patients do not respond or relapse after treatment. Here, we analyzed the therapeutic potential of the tumor suppressor microRNA-28 (miR-28) for DLBCL, alone and in combination with the Bruton's tyrosine kinase inhibitor ibrutinib. Combination therapy with miR-28 plus ibrutinib potentiated the anti-tumor effects of monotherapy with either agent by inducing a specific transcriptional cell-cycle arrest program that impairs DNA replication. The molecular actions of miR-28 and ibrutinib synergistically impair DNA replication by simultaneous inhibition of origin activation and fork progression. Moreover, we found that downregulation of the miR-28-plus-ibrutinib gene signature correlates with better survival of ABC-DLBCL patients. These results provide evidence for the effectiveness of a new miRNA-based ibrutinib combination therapy for DLBCL and unveil the miR-28-plus-ibrutinib gene signature as a new predictor of outcome in ABC-DLBCL patients.

Cell Death and Disease (2023)14:687 ; https://doi.org/10.1038/s41419-023-06178-0

INTRODUCTION

Diffuse large B cell lymphoma (DLBCL) is the most common aggressive lymphoma and accounts for nearly 40% of B cell non-Hodgkin lymphomas (B-NHL) [1]. DLBCL shows heterogeneous clinical manifestations and responses to therapy [1]. The disease was initially classified according to gene expression profiles into two major subtypes, called germinal center B cell-like (GCB) DLBCL and activated B cell-like (ABC) DLBCL [2]. Gene expression in GCB-DLBCL is characteristic of normal germinal center (GC) B cells, whereas ABC-DLBCL has post-germinal center features and expresses genes that are induced following B cell receptor (BCR) engagement and B cell activation. A major hallmark of ABC-DLBCL is activation of the NF-*k*B pathway [3]. Genetic profiling has provided a deeper understanding of the heterogeneous genetic aberrations in DLBCL, resulting in the identification of four DLBCL subtypes termed MCD, BN2, N1, and EZB, which differ not only in their genetic alterations but also in their gene expression signatures and clinical outcomes [4].

About 60% of DLBCL patients are cured by chemotherapy with rituximab plus cyclophosphamide, doxorubicin, vincristine, and prednisone (R-CHOP) [5, 6]. However, ABC-DLBCL has a worse prognosis than GCB-DLBCL [2, 7], and disease progression after R-CHOP chemotherapy is prevented in only 40% of ABC-DLBCL patients [1, 7]. Moreover, most patients who relapse or are refractory to initial therapy succumb to their disease [8]. New drug development for DLBCL patients over the past decade has focused on identifying specific, more effective, and non-cytotoxic targeted therapies [1, 9]. A major advance in DLBCL therapy development can be achieved with the advent of ibrutinib, a Bruton's tyrosine kinase (BTK) inhibitor that blocks B-cell receptor (BCR) dependent NF-*k*B activation and is approved for the treatment of mantle cell lymphoma, chronic lymphocytic leukemia, marginal zone lymphoma and Waldenström's macroglobulinemia [10, 11]. Clinical trials have shown that ibrutinib is especially effective when used in combination with R-CHOP to treat young ABC-DLBCL patients of the MCD and N1 genetic subtypes [12, 13]. However, DLBCL patients are often elderly and have age-related comorbidities, and therefore there is a need for new non-chemotherapy-based combination regimens that enhance the response to ibrutinib.

microRNAs (miRNAs) are non-coding RNAs that negatively regulate gene expression. Through imperfect base pairing, miRNAs bind to their target mRNAs and promote their degradation or translational blockade. Each miRNA binds numerous target mRNAs, regulating the expression of gene networks [14]. miRNA expression is frequently dysregulated in cancer, and miRNAs have been shown to play a causative role in B cell lymphoma development, acting as tumor suppressors or tumor promoting OncomiRs [15]. miRNA-based therapeutics is envisioned as an attractive alternative approach for B-NHL and other cancers (reviewed in [16] and [17]). We previously reported that miR-28 is a tumor suppressor miRNA that regulates a BCR-dependent signaling network in B cells [18, 19]. Here, we have assessed the

[1]B Cell Biology Laboratory Centro Nacional de Investigaciones Cardiovasculares (CNIC), Madrid, Spain. [2]Department of Immunology, Ophthalmology and ENT, Universidad Complutense de Madrid; Instituto de Investigación Sanitaria Hospital 12 de Octubre (imas12), Madrid, Spain. [3]DNA replication Group. Centro Nacional de Investigaciones Oncológicas (CNIO), Madrid, Spain. [4]Comparative Medicine Unit. Centro Nacional de Investigaciones Cardiovasculares (CNIC), Madrid, Spain. [5]These authors contributed equally: Almudena R. Ramiro, Virginia G. de Yébenes. ✉email: aramiro@cnic.es; vgarciay@ucm.es

Edited by Marco Herold

Received: 30 November 2022 Revised: 7 September 2023 Accepted: 26 September 2023
Published online: 18 October 2023

therapeutic value of miR-28 for DLBCL alone and in combination with ibrutinib. We present evidence that miR-28 enhances the anti-tumor effect of ibrutinib, promoting a specific gene expression program that inhibits DNA replication and cell proliferation in DLBCL.

MATERIALS AND METHODS

Cell culture

Human DLBCL cell lines (DOHH2, DB, OCI Ly19, MD-901, RIVA, U2932, HBL1, and SUDHL4) were grown at 37 °C in the presence of 5% CO_2 and maintained in RPMI supplemented with 10% fetal bovine serum, 1% penicillin/streptomycin, and 10 mM Hepes (Gibco). All cell lines were regularly tested for mycoplasma with the MycoAlert PLUS Mycoplasma Detection Kit (Lonza).

Isolation of human B cell subsets from tonsils

Tonsil samples and data from donors included in this study were provided by the Hospital Universitario Puerta de Hierro Majadahonda (HUPHM)/Instituto de Investigación Sanitaria Puerta de Hierro-Segovia de Arana (IDIPHISA) Biobank (Carlos III Health Institute Biobanks and Biomodels Platform) and were processed following standard operating procedures with the appropriate approval of the Ethics and Scientific Committees (AC0123-A-2023). Informed consent was obtained from all subjects. Human tonsils were taken during routine tonsillectomy. Tonsils were first minced, and the resulting cell suspension was subjected to Ficoll-Paque (Merck-Sigma Aldrich; GE17-1440-02) density centrifugation following manufacturer's instructions. Isolated lymphocytes were stained with fluorophore anti-human antibodies to detect CD19 (Cat#555415, clone HIB19), CD38 (Cat#562444, clone HIT2), IgD (Cat#348210, clone IA6-2) and CD27 (Cat#555441, clone M-T271). Naïve B cells ($CD19^+CD27^-IgD^+CD38^-$), GC ($CD19^+IgD^-CD38^+$) and post-GC memory B cells ($CD19^+CD27^+CD38^{-/lo}$) were isolated with a FACSFusion Cell Sorter.

Mice

Nonobese diabetic severe combined immunodeficiency G (NOD/SCID/IL-2rynull; NSG) mice were housed in the Centro Nacional de Investigaciones Cardiovasculares (CNIC) animal facility under specific pathogen-free conditions. All animal procedures conformed to EU Directive 2010/63EU and Recommendation 2007/526/EC regarding the protection of animals used for experimental and other scientific purposes, enacted in Spanish law under RD 53/2013. Animal procedures were reviewed by the CNIC Institutional Animal Care and Use Committee (IACUC) and approved by the Consejeria de Medio Ambiente, Administración Local y Ordenación del Territorio of the Comunidad de Madrid. Allocation of mice and samples into groups was random. Data acquisition was performed blindly, when technically possible.

Lymphoma models

For subcutaneous (SC) xenografts, $1–5 \times 10^6$ DOHH2, DB, OCI Ly19, MD-901, RIVA, U2932 or SUDHL4 cells were mixed in a 1:1 in Matrigel (BD Biosciences)/PBS and injected into the flanks of 10-week-old NSG mice. In mice injected with transduced MD-901, SUDHL4 or U2932 cells, doxycycline (Sigma-Aldrich) was administered twice per week at 0.04% in the drinking water, and mice received daily 40 mg/kg intraperitoneal (IP) injections or 20 mg/kg oral gavage administrations of ibrutinib (PCI-32765) (MedChemExpress) from day 10–12 after the SC xenograft. For IP administration, ibrutinib was dissolved in 10% DMSO and 90% corn oil. For oral gavage administration, ibrutinib was dissolved in 5% DMSO, 30% polietilenglicol 300, 5% Tween 80 and 60% water. 200 µl of either solution was administered to each mouse. Untreated groups were administered with vehicle.

The ABC-DLBCL Patient Derived Xenograft DFBL-18689-V2 was obtained from the public repository of xenografts of the Dana-Faber Cancer Institute under patient-derived material transfer agreement number A11877. To establish subcutaneous DFBL-18689-V2 PDX tumors, NSG mice received intravenous (IV) injections of DFBL-18689-V2 PDX cells, and splenocytes were extracted after 23–28 days. $1–3 \times 10^6$ cells were resuspended in PBS, mixed with 30–50% matrigel, and injected SC into the flanks of 6–8-week-old NSG.

Subcutaneous tumor volume was measured with a digital caliber using the following formula: volume = $(\text{width})^2 \times \text{length}/2$. Tumor growth was calculated for each individual tumor as the tumor volume at the indicated time point normalized to the initial tumor volume (at the time of starting treatment).

Treatment with miR-28 mimics

miRNA mimics of miR-28 and the scramble control sequence were purchased from Ambion. Established DFBL-18689-V2 PDX tumors (>100 mm^3) or DLBCL tumors (>150 mm^3) were treated with weekly intratumor injections of 0.5 nmol miRNA mimics (miR-28 or control) together with invivofectamine (Ambion).

FACS analysis of DFBL-18689-V2 PDX cells

DFBL-18689-V2 was acquired from the Public Repository of Xenografts (PRoXe). PDX cells ($0.25–1 \times 10^6$) were injected IV into 6–8-week-old NSG mice, and mice were sacrificed on day 26–31 after injection. Single-cell suspensions were obtained from spleens, and erythrocytes were lysed (ACK Lysing Buffer). Cells were stained with combinations of the following antibodies: anti-mouse CD45-APC (Cat#559864, clone 30-F11), anti-mouse CD45.1-V450 (Cat#560520, clone A20), anti-mouse CD45.2-V450 (Cat#560697, clone 104) anti-human IgM-APC (Cat#551062, clone G20-127), anti-human CD20-FITC (Cat#555622, clone 2H7), and anti-human CD19-APC (Cat#555415, clone HIB19) (all from BD Pharmigen). For proliferation analysis, cells were fixed and permeabilized using the Intracellular Fixation and Permeabilization Buffer Set (eBiosience) and stained with anti-ki67 (Abcam; Cat#ab16667); staining was revealed with alexa fluor 647 goat anti-rabbit IgG (H + L) (L.T.) (ThermoFisher, A-21245). Live cells were detected with DAPI (Sigma-Aldrich) or with LIVE/DEAD Fixable Yellow Dead Cell Stain (Thermo Fisher, L34959). Labeled cells were acquired with a LSRFortessa High-Parameter Flow Cytometer and analyzed with FlowJo V10.4.2 software.

DFBL-18689-V2 PDX transcriptome analysis

DFBL-18689-V2 PDX SC tumors were treated by intratumoral injection with 0.5 nmol of miR-28 or control mimics. Three independent pairs of DFBL-18689-V2 PDX tumors treated with miR-28 or control obtained at day 5 after the mimic treatment were used for RNA-seq. Total RNA was used to generate barcoded RNA-seq libraries using the NEBNext Ultra RNA Library preparation kit (New England Biolabs). First, poly A + RNA was purified using poly-T oligo- attached magnetic beads followed by fragmentation and first and second cDNA strand synthesis. Next, cDNA ends were repaired and adenylated. The NEBNext adaptor was then ligated followed by Uracile excision from the adaptor and PCR amplification. Libraries were sequenced on a HiSeq2500 (Illumina) to generate 60 bases single reads. FastQ files for each sample were obtained using CASAVA v1.8 software (Illumina). Differential expression between miR-28- and control-treated tumors was analyzed by ANOVA (314 protein coding transcripts, p-value < 0.05), and expression values were presented in a heatmap.

Alterations to disease and functions in miR-28- and control-treated tumors were identified by Ingenuity pathway analysis (IPA) of differentially expressed genes (DEGs) (p-value < 0.05).

Gene set enrichment analysis and gene signature analysis

The miR-28–induced transcriptome profile in the DFBL-18689-V2 PDX model was compared with the DLBCL gene signature through a Geo2R analysis of raw data from GEO GSE44337 [20]. For the differential expression analysis between DLBCL and PB B-cells, we used DLBCL samples (GSM1083475, GSM1083476, GSM1083477, GSM1083478, GSM1083479, GSM1083480, GSM1083481, GSM1083482, and GSM1083483) and human peripheral blood B-cells (GSM1083472, GSM1083473, and GSM1083474). Data were filtered for an adjusted p-value < 0.05 and log fold change (FC) < −1.5 or >1.5, and the DLBCL gene signature was obtained as logFC >1.5. Enrichment of the DLBCL gene signature in the RNA-seq data from miR-28–treated PDX tumors was tested by Gene Set Enrichment Analysis (GSEA).

For a more specific characterization of the pathways altered by the combined action of miR-28 and ibrutinib in MD-901 cells, GSEA was performed to determine whether there was enrichment of Reactome gene sets. The rank list used for this analysis was the DEG analysis comparing miR-28+ibrutinib versus control.

ABC-DLBCL patients with outcome data [4] were ranked using singscore [21, 22] according to their enrichment score for the miR-28+ib signature (downregulated genes) before R-CHOP treatment.

Lentiviral expression constructs

Lentiviral constructs were generated to transduce the human DLBCL cell lines HBL1, MD-901, U2932, and SUDHL4. The miR-28 precursor sequence was cloned into the doxycycline-inducible pTRIPZ vector (Thermo

scientific), and a scramble pTRIPZ vector was used as a control. Lentiviral supernatants were obtained 48 h after transfection of 293 T cells with packaging vectors (VSVG, Δ9.8) and pTRIPZ plasmids. Transduced human lymphoma cell lines were selected by culture in the presence of 0.4 µg/ml puromycin for 3 days. Expression of miR-28 or the scramble control sequence was induced by exposure to 0.5 µg/ml doxycycline for 2 days. Transduced RFP+ cells were isolated with a FACS Aria cell sorter for subsequent experiments.

miR-28+ ibrutinib combined treatment analysis in vitro

Human DLBCL cells (HBL1, MD-901, U2932 and SUDHL4) transduced with pTRIPZ-miR-28 or pTRIPZ-scramble were counted, and 200,000 cells were seeded in duplicate on a 48-well plate in fresh medium containing doxycycline at 0.5 µg/ml to induce miRNA expression. Serial dilutions of ibrutinib (Selleck Chem) were prepared in vehicle (DMSO), and equal volumes of the diluted drug were added to cells to achieve the desired final concentration. At least two independent experiments were performed per cell line. The number of viable cells was determined 72 h after the start of ibrutinib treatment using CellTiter-Glo® reagent. Luminescence was measured with an Orion Plate Luminometer reader (Berthold). Luminescence values in medium-only wells were subtracted to yield relative luminescence units (RLU), and the data were normalized to DMSO-treated or ibrutinib-treated control cells. The percentage of apoptotic (Annexin V^+ $Dapi^-$) or dead ($Dapi^+$) cells was measured 72 h after ibrutinib treatment by Annexin V (Biolegend, Cat#640932) and Dapi staining, and RFP expression was measured by flow cytometry in an LSRFortessa High-Parameter Flow Cytometer and analyzed with FlowJo V10.4.2 software.

miR-28+ibrutinib combined treatment transcriptome analysis

SUDHL4, U2932 or MD-901 cells transduced with pTRIPZ-scramble or pTRIPZ-miR-28 were induced with doxycycline (0.5 µg/ml) for 24 h. Cells were then seeded at 200,000 cells/ml and treated with ibrutinib (3 µM for SUDHL4 and 25 µM for U2932 and MD-901), while maintaining doxycycline in the medium. As a control, cells were treated with vehicle (DMSO). RFP+ cells were isolated in a FACS Aria cell sorter at 0, 4, or 20 h after the start of ibrutinib treatment ($n = 2$). RNA was extracted from RFP+ sorted cells using miRNeasy mini kit (Qiagen). Transduced MD-901 SC tumors were treated with doxycycline in the drinking water and IP injections of ibrutinib. Three independent pairs of MD-901 tumors treated with ibrutinib, miR-28, miR-28+ibrutinib or control were used for RNA-seq. RNA was extracted using miRNeasy mini kit (Qiagen). Total RNA was used to generate barcoded RNA-seq libraries using the NEBNext Ultra II Directional RNA Library preparation kit (New England Biolabs) according to manufacturer's instructions. First, poly A + RNA was purified using poly-T oligo- attached magnetic beads followed by fragmentation and first and second cDNA strand synthesis. Next, cDNA ends were repaired and adenylated. The NEBNext adaptor was then ligated followed by second strand removal, uracile excision from the adaptor and PCR amplification. Libraries were sequenced on a HiSeq4000 (Illumina) to generate 60 bases single reads. FastQ files for each sample were obtained using bcl2fastq 2.20 Software (Illumina). Differential expression analysis was performed with the Limma R package at the different time points (0, 4, or 20 h) and also time-independently for MD-901 cells. The RNA-seq data of the manuscript is available at the GEO Repository (GSE229788).

miR-28+ib signature

The miR-28+ib signature was obtained through differential expression (DE) analysis of RNA-seq data from pTRIPZ-transduced MD-901 cells expressing miR-28 or the control scramble sequence and exposed to vehicle (DMSO) or ibrutinib for 20 h, yielding three experimental conditions: single treatment with miR-28, single treatment with ibrutinib, and combined treatment with miR-28+ibrutinib. All analyses were filtered for an adjusted p-value < 0.05. Three overlap analyses were performed to obtain the miR-28+ib signature, defined as genes that changed with the combined treatment but not with the single treatments. First, to exclude genes that change with ibrutinib treatment, an overlap analysis was performed between DEGs obtained with the comparison of miR-28+ibrutinib versus miR-28 and ibrutinib versus control; since there was no overlap, the whole set of 455 genes was included in 'list 1'. Second, to exclude genes that change with miR-28 treatment, an overlap analysis was performed between DEGs obtained with the comparison of miR-28+ibrutinib versus ibrutinib and miR-28 versus control; the overlapping 3290 genes were eliminated, and the remaining 1437 genes were assigned to 'list 2'. Third, an overlap analysis was performed between list 1 and list 2, and the resulting list of 157 overlapping genes was defined as the miR-28+ib signature (Fig. S3B).

GO terms were assigned to each gene in the signature. A heatmap was generated to represent the Z-score expression values of the 157 genes in miR-28+ib signature for the different treatments and time points, and the 7 most representative GO terms were depicted.

Ingenuity Pathway Analysis (IPA) was used to identify the distinct signaling pathways and networks in miR-28+ib signature. Two merged DNA replication-related networks identified with IPA were represented using STRING tool.

Comparative ingenuity pathway analysis

To analyze signaling pathways altered by the single and combined treatments, a comparative IPA was performed with the following three time-independent differential expression analysis for MD-901 cells (filtered for an adjusted p-value < 0.05 and logFC <−1 or >1): miR-28 versus control, ibrutinib versus control, and miR-28+ibrutinib versus control. For SUDHL4 and U2932 cells and MD-901 tumors, all DEGs (adjusted p-value < 0.05) between the combined treatment (miR-28+ibrutinib) and untreated controls were used as input for the comparison pathway analysis. Diseases and functions related to cell cycle and proliferation were compared between cell lines. P-values were corrected for multiple testing using the Benjamini-Hochberg (B–H) false discovery rate. Positive and negative Z-scores predict the activation or inhibition of the pathway, respectively.

Cell proliferation

MD-901 and SUDHL4 cells transduced with pTRIPZ-scramble or pTRIPZ-miR-28 were induced with doxycycline (0.5 µg/ml) for 24 h. Cells were then plated at 200,000 cells/ml and treated with the indicated ibrutinib concentrations in medium containing doxycycline. After 20 h, the cell cycle was analyzed using DAPI staining and the FITC BrdU Flow kit (BD Pharmigen, Cat#559619). The sub G0-G1 population was determined in DAPI-negative gated cells.

Histopathology

Tumors were fixed in formalin and embedded in paraffin. Sections were cut and stained with hematoxylin and eosin (Sigma) or anti-Ki-67 (rabbit polyclonal antibody, Life Technologies, Thermofisher, PA5-19462). Ki-67 positive lymphoma areas were quantified on scanned slides using NDP.view2 plus software. Two outliers were removed with iteractive Grubbs' analysis (alpha = 0.1) in Graphpad Prism.

Protein detection by immunoblot

Control and miR-28-pTRIPZ-transduced MD-901 cells were induced with doxycycline, plated at 200,000 cells/ml, and treated for 20 h with 25 µM ibrutinib with doxycycline in the medium. Whole cell extracts were prepared by cell resuspension in Laemmli buffer (50 mM Tris–HCl pH 6.8, 10% glycerol, 3% SDS, 0.006 w/v bromophenol blue, 5% 2-mercaptoethanol) followed by sonication (3 × 4 s) in a Branson Digital Sonifier set at 50% amplitude. Immunoblots were performed using standard protocols. Primary antibodies used in this study: anti-CDC45 (generated in Méndez Lab, 1:1000; [23]), anti-CDC7 (Novus Biologicals NB120-17880, 1:1000), anti-PCNA (Proteintech 60097-1-Ig, 1:1000), anti-PSF1 (generated in Méndez Lab, 1:1000; [23]), anti-CHK1 (Santa Cruz Biotechnology sc-8408; 1:10,000), anti-Histone H3 (Abcam ab1791, 1:20,000). LI-COR secondary antibodies: IRDye 800CW goat anti-rabbit (926-32211) and IRDye 680RD goat anti-mouse (926-68070; LI-COR, Bad Homburg, Germany).

Single-molecule analysis of DNA replication

Control and miR-28 pTRIPZ-transduced MD-901 cells were induced with doxycycline, plated at 300,000 cells/ml, and treated for 20 h with 12.5 µM ibrutinib and doxycycline in the medium. Cells were pulse-labeled sequentially with 50 µM 5-chloro-2′-deoxyuridine (CldU; 20 min) and 250 µM 5-iodo-2′-deoxyuridine (IdU; 20 min). Labeled cells were lysed in 0.2 M Tris pH 7.4, 50 mM EDTA, 0.5% SDS. Stretched DNA fibers were prepared as described (Terret et al, 2009). For the immunodetection of labeled tracks, fibers were incubated with primary antibodies anti-CldU (rat monoclonal anti-BrdU, Abcam, AB6326), anti-IdU (mouse monoclonal anti-BrdU, BD Biosciences, 347580) and anti-ssDNA (mouse monoclonal IgG2a, Millipore MAB3034) for 1 h at RT in a humidity chamber, followed by incubation with Alexa Fluor-conjugated secondary antibodies (Invitrogen/

Molecular Probes, A-11007, A-21121, and A-21241) for 30 min at RT. Microscopy images were obtained with a DM6000 B Leica microscope equipped with an HCX PL APO 40×, 0.75 NA objective. A standard conversion rate of 1 µm = 2.59 kb was used [24]. Signals were measured and quantified using ImageJ software. For the analysis of fork rate, the length of the green track was measured in red–green structures (>300 tracks measured per condition and replicate). The frequency of origin activation was determined as the percentage of green–red–green structures (origins activated during the CldU pulse) relative to all replicative structures containing a red track, as described [25]. >500 structures were measured per condition and replicate. A conversion factor 1 µm = 2.59 kb was used [24].

microRNA quantification by RT-qPCR

RNA was extracted from FACS sorted naïve, GC and post-GC memory B cells of human tonsils, as well as from human DLBCL cell lines using miRNeasy mini kit (Qiagen). cDNA was synthesized using miRCURY LNA RT kit (Qiagen) and quantified by SYBR green assay (miRCURY LNA SYBR Green PCR Kit, Qiagen). For detection of human mature miR-28a-5p, the following miRCURY LNA miR-28 primer (Qiagen; Cat# 2YP00204322) was used. U6 amplification (Qiagen; Cat#YP00203907) was used as normalization control. Amplification was performed in QuantStudio5-384 Real-Time PCR System (Applied Biosystems) equipment.

Statistics

Sample sizes were chosen to provide confidence in the results and measurements, based on previous studies. Number of mice used in each experiment is indicated in figure legends and/or Methods. Statistical analyses were performed in GraphPad Prism 8 and are specified in figure legends. Error bars represent standard deviation or SEM of the mean, as indicated in the figure legends. Normality of the data was assessed with the Anderson-Darling test. Normally distributed data were analyzed using two-tailed unpaired Student t-*test* for comparison of two experimental groups or ANOVA for comparison of more than two groups. For xenograft experiments comparing the tumor volume and growth of two or more groups over time, linear mixed effects regression models [26] run with R software package lme4 (v1.1-30) were used (tumor volume/growth value ~ treatment*day + (1| tumor id), data = dataset). Treatment and day were specified as fixed terms. Tumor id factor was used as random effect for slope. Model was built with interaction between fixed factors. Differences were assessed by comparing estimated mean value of each treatment condition at each day. Differences were computed using Emmeans (v1.7.5) and tests were performed using lmerTest (v.3.1-3) packages. Not normally distributed data was analyzed with Kruskal–Wallis test and Dunn's post-test. Differences were considered significant at p-values < 0.05.

RESULTS

miR-28 inhibits DLBCL tumor growth

To evaluate the anti-tumor activity of miR-28 in treatment-refractory B cell lymphoma, we used different DLBCL models. First, we quantified miR-28 expression in a collection of DLBCL cell lines, which included four GCB-DLBCL (DOHH2, OCI Ly19, SUDHL4 and DB) and four ABC-DLBCL (U2932, HBL1, MD-901 and Riva), and in three primary human B cell subsets: naïve, GC and post-GC memory B cells. Within primary B cells, miR-28 expression was highest in GC B cells, in agreement with previous reports [27, 28]. Comparison of DLBCL cell lines and GC B cells showed that all the DLBCL cell lines analyzed have reduced miR-28 levels (Fig. 1A). Thus, human DLBCL cell lines faithfully recapitulate the down-regulation of miR-28 expression described in primary DLBCL samples and other GC-derived neoplasms [18, 19, 29, 30]. Using human DLBCL xenografts, we assessed the anti-tumor activity of a synthetic miR-28 analog (mimic) [31]. Three GCB-DLBCL (DOHH2, OCI Ly19, and DB) and three ABC-DLBCL (U2932, MD-901, and Riva) human cell lines were injected subcutaneously into NOD *scid* gamma (NSG) mice. Tumors were allowed to reach at least 150 mm^3, and mice were then treated with intratumoral injections of 0.5 nmol miR-28 or control mimics (Fig. S1A). The synthetic miR-28 mimic significantly inhibited tumor growth of all six human DLBCL cell lines tested, with similar efficacy in the ABC-DLBCL and GCB-DLBCL cell lines (Fig. 1B, C). We next used a patient-derived xenograft (PDX) ABC-DLBCL model from the PRoXe xenograft repository [32]. This PDX was isolated from an untreated patient and is characterized by the expression of human CD19, CD20, and IgM and by high expression of the Ki-67 proliferation marker when injected into NSG mice (Fig. 1D). The synthetic miR-28 mimic significantly inhibited the tumor growth of DLBCL PDX xenografts after two administrations (Fig. 1E, S1B). RNA-seq transcriptome analysis of ABC-DLBCL PDX tumors 5 days after treatment with the scramble miRNA (control) or the miR-28 mimic (3 tumors per treatment) revealed miR-28-induced expression changes in 314 protein-coding transcripts (Fig. 1F, Table S1A). Ingenuity Pathway Analysis (IPA) showed that miR-28 coordinately inhibited the expression of gene networks implicated in tumor growth (Fig. 1G, Table S1B). Tumoral growth and B cell signaling gene networks were also inhibited in miR-28 expressing MD-901 ABC-DLBCL tumors (Fig. S1C, D). In addition, Gene Set Enrichment Analysis (GSEA) showed that miR-28 significantly downregulated transcripts in ABC-DLBCL PDX tumors known to be overexpressed in DLBCL patients ($p = 0.026$, NES = −1.13) (Fig. 1H). Together, these results show that synthetic miR-28 analogs inhibit DLBCL growth in vivo through the downregulation of gene networks involved in tumor growth.

miR-28 potentiates the anti-tumor effect of ibrutinib

We next investigated whether miR-28 can sensitize DLBCL to the BTK inhibitor ibrutinib. We first tested in vitro cell viability and growth in the presence of ibrutinib after the induction of miR-28 expression in four human DLBCL cell lines. Three ABC-DLBCL (MD-901, U2932 and HBL1) cell lines and one GCB-DLBCL (SUDHL4) cell line were transduced with a doxycycline-inducible lentiviral vector encoding miR-28 (pTRIPZ-miR-28) or a scramble sequence (pTRIPZ-scramble) together with red fluorescent protein (RFP) (Fig. S2A). We first tested ibrutinib sensitivity in each control-transduced cell line, as analyzed 3 days after ibrutinib treatment. Cell viability was quantified as the total number of viable cells measured by CellTiter-Glo® luminescent ATP detection assay (Fig. 2A) and as the proportion of apoptotic and dead cells stained with Annexin V and the Dapi DNA-dye, detected by flow cytometry (Fig. S2B). Ibrutinib caused a reduction in the total number of viable cells and promoted cell death at different concentrations in the four cell lines (Fig. 2A and S2B). As expected, the highest sensitivity was detected in HBL1 cells, which harbor MYD88 L265P and CD79B mutations that confer high sensitivity to ibrutinib [33]. In all four DLBCL cell lines tested, doxycycline-induced miR-28 expression reduced the total number of viable cells upon ibrutinib treatment (Fig. 2A) but resulted in no significant changes in the proportion of apoptotic (Annexin V^+ $Dapi^-$) or dead ($Dapi^+$) cells (Fig. S2B). The enhancement of ibrutinib anti-tumor activity in the presence of miR-28 differed among the different cell lines, with the strongest effect detected in MD-901 cells (Fig. 2A). We next assessed the ability of miR-28 to enhance the anti-tumor effect of ibrutinib on the growth of DLBCL xenografts in vivo. MD-901 cells transduced with pTRIPZ-miR-28 or pTRIPZ-scramble were injected subcutaneously into NSG mice, and once tumors were detectable, mice were given doxycycline in the drinking water for 8 days to induce miR-28 or scramble expression. During the same period, mice received daily intraperitoneal injections of ibrutinib or vehicle. There were thus four treatment groups: scramble alone (control); scramble plus ibrutinib; miR-28 alone; and miR-28+ibrutinib combination therapy. Induced miR-28 expression significantly enhanced the inhibitory effect of ibrutinib on MD-901 ABC-DLBCL tumor volume, growth and weight (Fig. 2B, S1E and Table S2A, B). Additionally, we performed miR-28 and ibrutinib monotherapy and combined treatments in U2932 and SUDHL4 xenografts, establishing the same four treatment groups. We found that in both U2932 (Fig. 2C, Table S2C) and SUDHL4 (Fig. S1F) xenografts, miR-28+ibrutinib therapy inhibits DLBCL

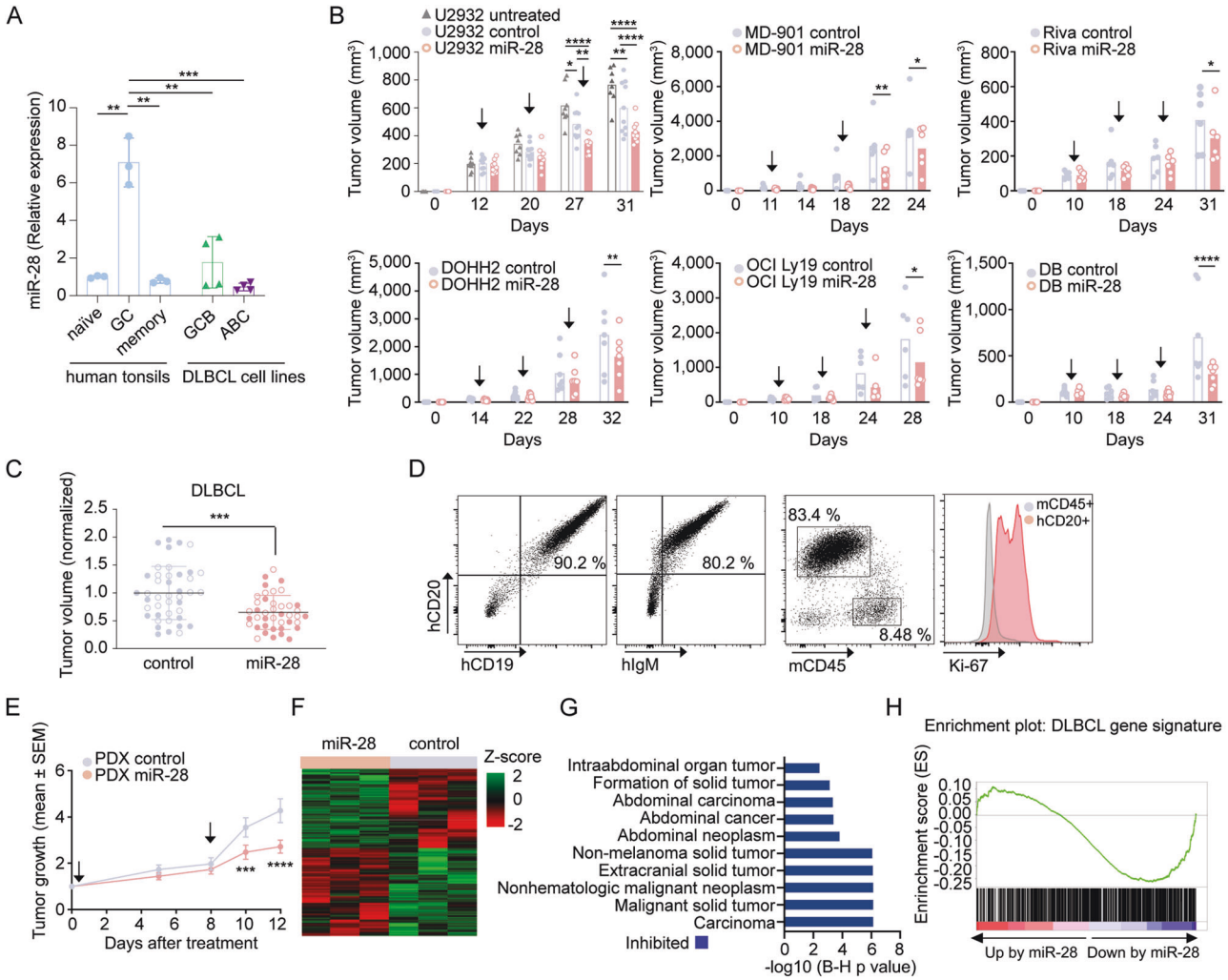

Fig. 1 miR-28 inhibits DLBCL tumor growth. A Quantification of miR-28 expression in primary human B cell subsets isolated from tonsils and in GCB-DLBCL and ABC-DLBCL cell-lines by qRT-PCR. The expression was normalized to the mean expression in naïve primary B cells ($CD19^+CD27^-IgD^+CD38^-$: 1 ± 0.6). Values indicate mean ± SD or the quantification in each cell line: GC ($CD19^+IgD^-CD38^+$: 7.1 ± 1.3), post-GC memory B cells ($CD19^+CD27^+CD38^{-/lo}$: 0.8 ± 0.5), GCB-DLBCL cell lines (1.8 ± 1.3: DOHH2 (3.2), OCI Ly19 (2.8), SUDHL4 (0.55), DB (0.63)) and ABC-DLBCL cell lines (0.46 ± 0.2: U2932 (0.29), HBL1 (0.71), MD-901 (0.30) and Riva (0.54)). **B**, **C** Tumor volume of ABC-DLBCL and GCB-DLBCL cell-line xenografts in NSG mice treated intratumorally with 0.5 nmol miRNA mimics: miR-28 (pink circles), scramble control (gray circles) or untreated (gray triangles). **B** ABC-DLBCL xenografts (upper graphs): U2932 ($n = 10$), MD-901 ($n = 6$), Riva ($n = 6$). GCB-DLBCL xenografts (bottom graphs): DOHH2 ($n = 7$), OCI Ly19 ($n = 6$), DB ($n = 7$). Bar plots show tumor volume at the indicated time points after DLBCL cell line xenograft injection. Arrows indicate dosing schedules. $^*P < 0.05$, $^{**}P < 0.01$, $^{****}P < 0.0001$, linear mixed model. **C** End-point tumor volume normalized to the mean volume in each control group for the xenografts shown in (**B**) (ABC-DLBCL, open circles; GCB-DLBCL, filled circles). $^{**}P < 0.01$, unpaired *t* test. **D** Representative flow cytometry plots of spleen-derived PDX cells (CD20+, CD19+, IgM+, mouse CD45-, Ki-67+) 26 to 31 days after infusion of PDX cells in NSG mice. **E**–**H** Effect of miR-28 on tumor growth in a DLBCL–patient-derived xenograft (PDX) mouse model (PRoXe DFBL-18689-V2). **E** ABC-DLBCL PDX tumors were treated after reaching a medium volume ≥100 mm^3 (15 to 24 days after PDX injection) with intratumoral injections of 0.5 nmol miR-28 mimics or control. Tumor growth was calculated as tumor volume at the indicated time points normalized to the initial tumor volume prior treatment (mean ± SEM; $n = 24$ tumors, 3 independent experiments). Arrows indicate dosing schedules. $^{***}P < 0.001$, $^{****}P < 0.0001$, linear mixed model. **F** RNA-seq analysis of ABC-DLBCL PDX tumors 5 days after a single miRNA mimic treatment ($n = 3$ miR-28, $n = 3$ control). The heatmap shows expression of the 314 genes found to be differentially expressed (ANOVA *p*-value < 0.05). **G** The graph shows the top 10 significantly changed Pathways identified by Ingenuity Pathway Analysis (IPA). Pathway activity prediction is shown with a color code (blue, inhibited by miR-28). P-values were corrected for multiple testing using the Benjamini-Hochberg (B–H) false discovery rate. **H** Gene Set Enrichment Analysis (GSEA) of a DLBCL gene signature [20] in miR-28-treated PDX tumors (FWER *p*-value = 0.025, FDR *q* value = 0.066, NES = −1.13).

growth. Together, these results demonstrate that miR-28 enhances DLBCL sensitivity to ibrutinib.

miR-28+ibrutinib combination therapy induces a specific transcriptional program that inhibits the cell cycle and DNA replication

To investigate the effect of miR-28+ibrutinib combination therapy on the DLBCL transcriptome, we conducted an RNA-seq analysis to compare gene expression profiles after monotherapy versus combined miR-28+ibrutinib treatment. MD-901 cells transduced with pTRIPZ-miR-28 or pTRIPZ-scramble were induced with doxycycline for 24 h before ibrutinib treatment. RNA-seq was performed on RFP+ cells isolated by flow cytometry after 0, 4 and 20 h of ibrutinib exposure (Fig. S3A). Gene expression changes were identified in response to miR-28 expression, ibrutinib treatment and miR-28+ibrutinib combination (Fig. S3C, Table S3).

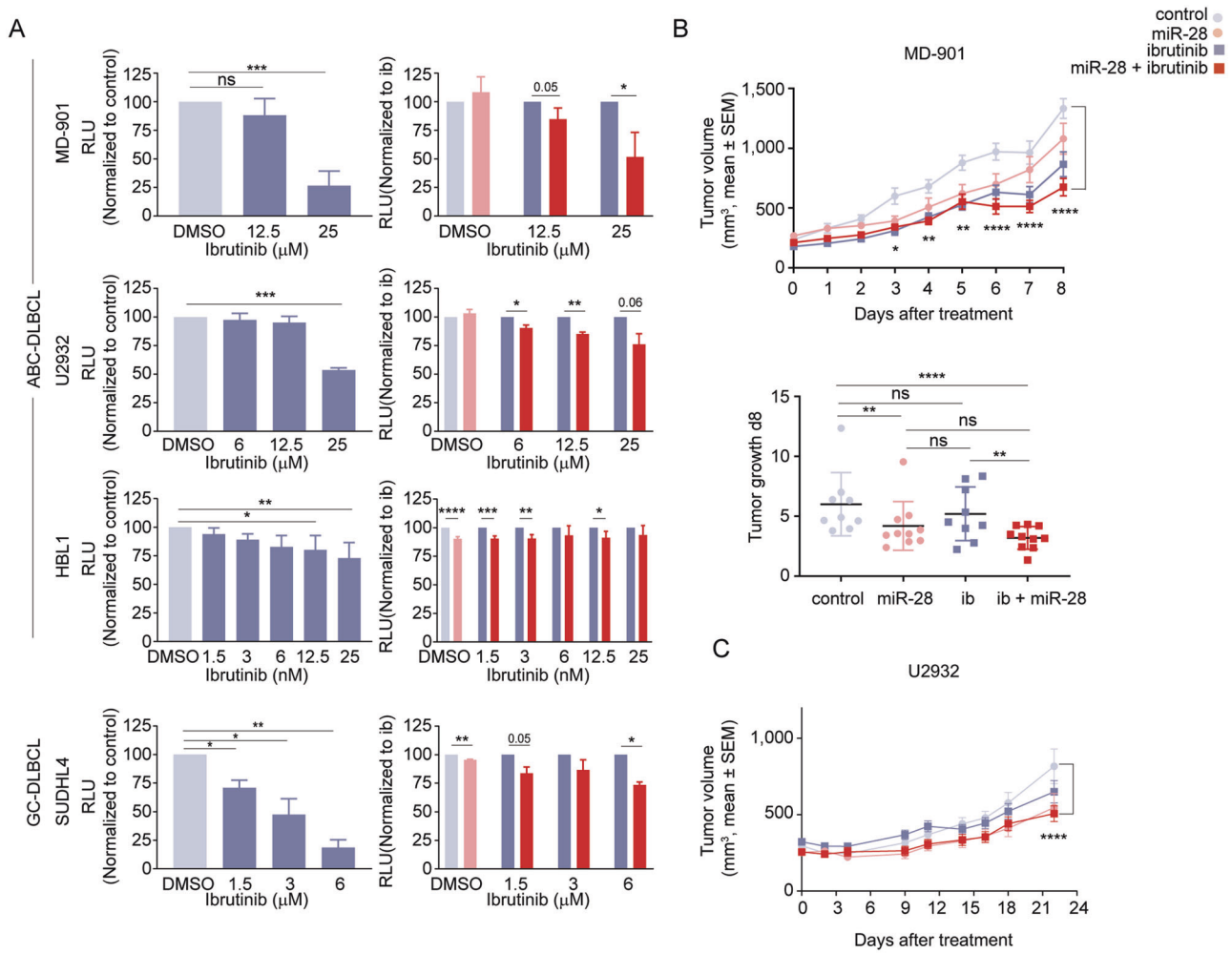

Fig. 2 miR-28 potentiates the anti-tumor effect of ibrutinib against DLBCL. A Effect of miR-28 on the growth of DLBCL cell lines treated with ibrutinib in vitro. DLBCL cell lines transduced with pTRIPZ-miR-28 (miR-28) or pTRIPZ-scramble (control) were treated with the indicated concentrations of ibrutinib in the presence of doxycycline. Viable cell number was determined at day 3 with CellTiter-Glo® reagent. Each row represents a different cell line: ABC-DLBCL subtype (upper rows: MD-901 ($n = 3$), U2932 ($n = 2$) and HBL1 ($n = 4$)); GCB-DLBCL subtype (lower row SUDHL4; $n = 2$). Error bars denote SD of n independent experiments. Left bar charts show sensitivity to ibrutinib in control cells, calculated as Relative Luminescence Units (RLU) normalized to control (control DMSO-treated, light gray; ibrutinib-treated, dark gray). Right bar charts show the effect of treatment with miR-28 plus ibrutinib (dark red) normalized to control cells for each ibrutinib concentration (dark gray). miR-28 cells normalized to control non-ibrutinib treated cells are shown in light pink. *$P < 0.05$, **$P < 0.01$, ***$P < 0.001$, ****$P < 0.0001$, unpaired *t* test. **B**, **C** Effect of miR-28+ibrutinib combination therapy on ABC-DLBCL xenografts growth in vivo. **B** Xenograft growth from MD-901 cells transduced with doxycycline-inducible pTRIPZ-miR-28 or pTRIPZ-scramble in NSG mice treated with daily intraperitoneal injections of ibrutinib (40 mg/kg) or vehicle and administered with doxycycline in the drinking water. The top graph shows tumor volume (mean volume ± SEM; $n = 5$ mice and 9–10 tumors per group). The lower graph shows tumor growth, calculated as tumor volume at day 8 normalized to initial tumor volume. *$P < 0.05$, **$P < 0.01$, ****$P < 0.0001$ vs control, linear mixed model. **C** Tumor volume of U2932 cells transduced with doxycycline-inducible pTRIPZ-miR-28 or pTRIPZ-scramble in NSG mice treated with daily administrations of ibrutinib (20 mg/kg) or vehicle via oral gavage and doxycycline in the drinking water ($n = 10$–12 tumors per group). Control (light gray circles), miR-28 (light pink circles), ibrutinib (dark gray squares), ibrutinib+miR-28 (dark red squares). ****$P < 0.0001$, linear mixed model. See Table S2 for complete statistical analysis.

This analysis identified a set of 157 genes (adjusted *p*-value < 0.05) that were significantly altered exclusively in MD-901 cells treated with miR-28+ibrutinib for 20 h, which we termed "miR-28+ib signature" (Fig. 3A, S3B and Table S4A). Genes in the miR-28+ib signature were mostly associated with DNA replication, DNA repair, and cell cycle pathways, and miR-28+ibrutinib combination therapy mostly resulted in their downregulation (Fig. 3A). Analysis of the 114 downregulated genes from the miR-28+ib signature showed that the combined miR-28+ibrutinib treatment induced larger changes in expression levels of these 114 genes than the miR-28 or the ibrutinib monotherapies. Further, the effect of miR-28+ibrutinib was higher than the additive effect of both monotherapies, calculated as the sum of the changes triggered by the miR-28 and the ibrutinib monotherapies (Fig. 3B, C). Thus, this analysis shows that miR-28+ibrutinib combination has a synergic effect on the downregulation of miR-28+ib signature. The four most downregulated genes upon combined miR-28+ibrutinib treatment were GINS1 (the gene encoding PSF1), RRM2 and UHRF1, all encoding proteins described to be required for DNA replication [34–41] (Fig. 3C). Consistent with these findings, IPA and GSEA showed that miR-28+ibrutinib combination therapy coordinately inhibited the activity of gene networks involved in cell cycle and chromosomal replication (Fig. 3D, S3D and Table S4B, C). In addition, STRING functional enrichment analysis identified a protein–protein interaction network composed of 65 proteins related to cell division whose expression was predominantly

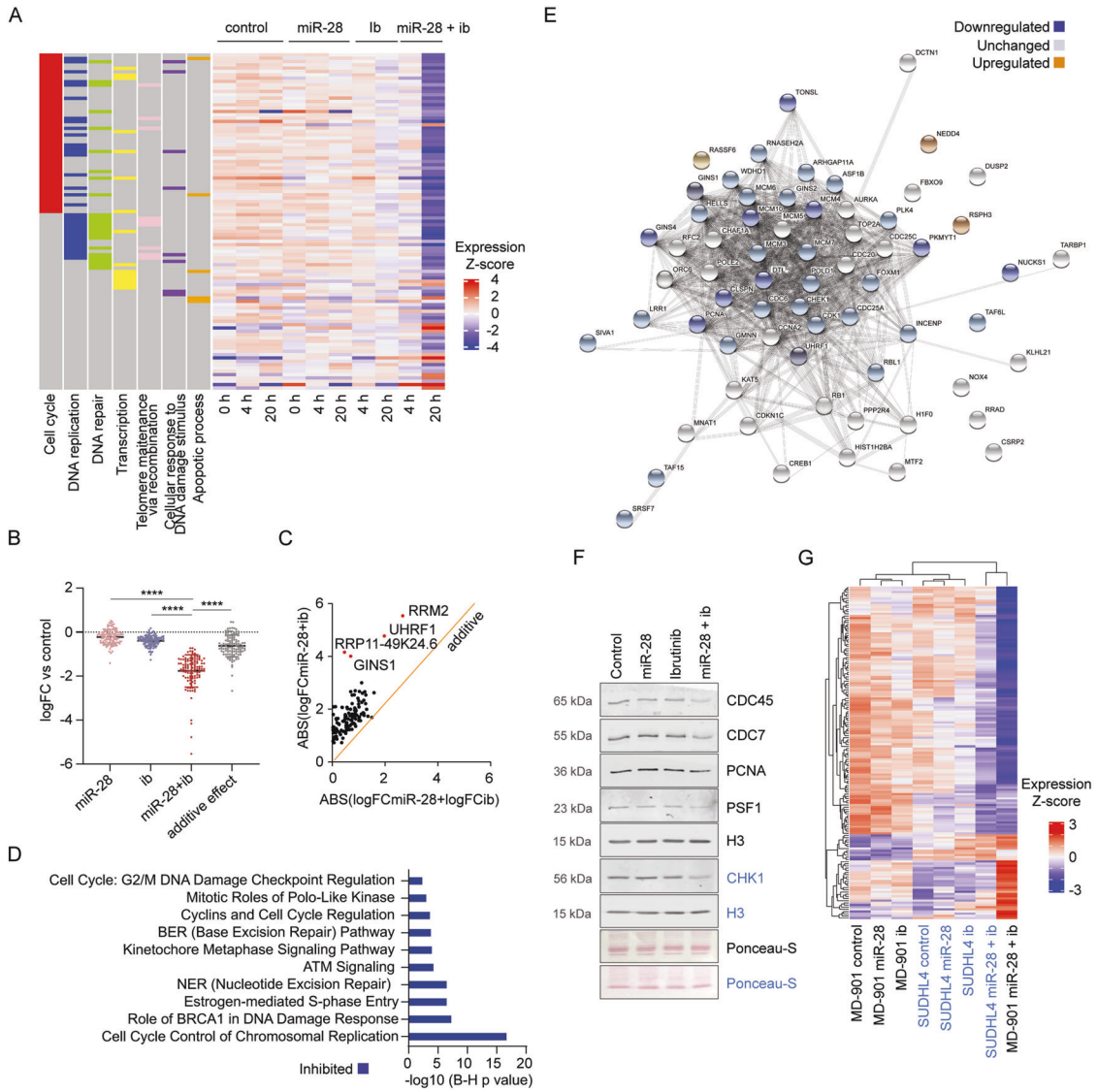

Fig. 3 Effect of miR-28 plus ibrutinib combined treatment on the DLBCL-cell transcriptome. Doxycycline-induced MD-901 or SUDHL4 cells transduced with pTRIPZ-miR-28 or pTRIPZ-control were treated with 25 or 6 μM ibrutinib, respectively. Whole transcriptome RNA-seq was performed in RFP^{+} cells isolated by flow cytometry after 0, 4, and/or 20 h of ibrutinib treatment. **A** Heatmap showing *Z*-score expression values for the 157 miR-28+ib signature genes in MD-901 cells at 0, 4 and 20 h in the four treatment conditions (control, miR-28, ibrutinib, and miR-28+ibrutinib). 114 genes were downregulated in the miR-28+ibrutinib condition. Columns on the left depict the 7 most representative Gene Ontology terms in the miR-28+ib signature. **B** Plot depicting expression changes as measured by log fold change (logFC) of the three treatment conditions (mono- and combination therapies) versus control MD-901 cells, and the expected theoretical values for additive effect of individual therapies. ****$P < 0.0001$, Kruskal–Wallis test and Dunn's post-test. **C** 114 downregulated genes of the miR-28+ib gene signature are represented as points relative to the calculated sum of the logFC of the individual treatments versus control (*x* axis) or the experimentally observed logFC of the combined therapy versus control (*y* axis). The orange line represents the location of theoretical additive expression values (slope = 1). Points above the line indicate synergy between treatments. The top 4 downregulated genes are highlighted. **D** Bar plot showing Benjamini-Hochberg (B-H) adjusted *p*-values for the top 10 Signaling Pathways in the miR-28+ib signature. Pathway activity prediction is shown with a color code (blue: inhibited by miR-28+ibrutinib combined treatment). **E** STRING protein-protein interaction network identified in the miR-28+ib signature by IPA. Upregulated proteins are depicted in orange, downregulated proteins in blue, and unchanged proteins in white. **F** Western blot analysis of selected replication proteins in doxycycline-induced pTRIPZ-miR-28– or pTRIPZ-scramble–transduced MD-901 cells after treatment for 20 h with 25 μM ibrutinib or DMSO. Histone H3 (H3) was used as loading control. Colors (blue and black) of protein letters indicate two different blots. Molecular weights of the proteins are shown in the left. **G** Hierarchical clustering heatmap showing *Z*-score expression values of the 157 miR-28+ib signature genes at 20 h in the four treatment conditions (control, miR-28, ibrutinib and miR-28+ibrutinib) in MD-901 and SUDHL4 cells.

downregulated upon miR-28+ibrutinib combination therapy (Fig. 3E).

Within this DNA replication and cell division network, we analyzed the expression of a selected set of proteins required for the formation and activation of DNA replication origins: (1) proteins of the pre-initiation complex (pre-IC) required for helicase activation and replisome assembly during the G1-S transition, including CDC45, CDC7, and PSF1, a subunit of the GINS complex; and (2) proteins recruited to functional replication forks after origin firing during S phase, such as PCNA and CHK1 [41]. This analysis revealed that miR-28+ibrutinib combination treatment caused a specific reduction in the expression levels of proteins

required for replication origin activation, including CDC45, CDC7, PSF1, PCNA, and CHK1, that were not observed in cells treated with miR-28 or ibrutinib individually (Fig. 3F, S4). Finally, we analyzed the impact of monotherapy and combined miR-28+ibrutinib treatment on gene expression profiles of two additional DLBCL cell lines, SUDHL4 GCB-DLBCL and U2932 ABC-DLBCL, by RNA-seq (Table S5A, B). We found that combined miR-28+ibrutinib treatment resulted in the inhibition of cell cycle proliferation and DNA replication pathways in SUDHL4 and U2932 cells (Fig. S3E and Table S5C), in agreement with our findings in MD-901 cells. Gene clustering analysis of the miR-28+ib signature genes in MD-901 and SUDHL4 cells showed that monotherapy treated cells cluster by cell type rather than by treatment condition. In contrast, the gene expression profile changes induced by combined miR-28+ibrutinib treatment in MD-901 and SUDHL4 clustered by treatment condition rather than by cell type (Fig. 3G). Accordingly, gene expression changes in U2932 cells treated with miR-28+ibrutinib also clustered with the miR-28+ib signature in MD-901 (Fig. S3F). These results reveal that the transcriptional program induced by combined miR-28+ibrutinib treatment is conserved in different DLBCLs, including both ABC and GCB subtypes. Together, these results indicate that miR-28+ibrutinib combination therapy induces a specific cell cycle and DNA replication inhibitory transcriptional program in DLBCL cells.

miR-28 potentiates the anti-tumor effect of ibrutinib against DLBCL by promoting cell cycle arrest

To analyze whether the transcriptional program induced by miR-28+ibrutinib combination therapy correlates with cell proliferation blockade, we first performed a pulsed BrdU and cell cycle analysis 20 h after ibrutinib treatment in miR-28–transduced MD-901 ABC-DLBCL and SUDHL4 GCB-DLBCL cells. For each cell line, we used two ibrutinib doses (Fig. 4A). When used individually as monotherapy, miR-28 and ibrutinib caused modest increases in the proportion of G_0/G_1 non-dividing cells and minor reductions in the proportion of BrdU-incorporating cells during S phase (Fig. 4A). In contrast, cell cycle inhibition was greatly enhanced by miR-28+ibrutinib combination (Fig. 4A). Inhibition of DNA replication observed upon combined therapy was greater in MD-901 ABC-DLBCL cells than in SUDHL4 GCB-DLBCL cells (Fig. 4A). The G2/M cell cycle phase was unaffected by either the individual therapies or the combined treatment. We did not observe differences in the fraction of subG0/G1 dead cells in miR-28+ibrutinib versus ibrutinib-only-treated DLBCL (Fig. 4B). Next, we performed RNA-seq analysis of MD-901 tumors 8 days after treatment (3 tumors per treatment condition) and found that cell cycle pathways were inhibited in miR-28- and miR-28+ibrutinib-treated tumors, although the inhibition was larger in miR-28+ibrutinib-treated tumors (Table S3H). Further, analysis of the Ki-67+ proliferative area of MD-901 ABC-DLBCL tumor xenografts revealed that only miR-28+ibrutinib combination therapy significantly reduced proliferation (Fig. 4C). Together, these results show that miR-28 potentiates the anti-tumor effect of ibrutinib by promoting DLBCL cell cycle arrest.

miR-28+ibrutinib combination therapy impairs DNA replication

To investigate the molecular mechanisms underlying the S-phase inhibition induced by miR-28+ibrutinib combined treatment, we monitored DNA replication in a stretched DNA fiber assay after sequential pulse-labeling of ABC-DLBCL cells with thymidine analogs CldU and IdU. This technique allows single-molecule resolution analysis of replicative dynamics through the quantification of fork progression rates and the frequency of active replication origins at a given time (Fig. 5A; [25]). MD-901 cells transduced with inducible miR-28 or scramble were treated with or without ibrutinib for 20 h. Both monotherapy treatments altered DNA replication dynamics (Fig. 5B–D): miR-28 monotherapy caused a 50% reduction in the number of active origins and a concomitant two-fold increase in fork rate; in contrast, ibrutinib monotherapy decreased fork rate by 30% while increasing by 20% the number of active origins. Origin activity and fork rate are related parameters: alterations that slow down forks lead to the activation of more origins as a compensatory mechanism [42, 43], whereas alterations that primarily increase origin number lead to lower fork rates, likely due to competition for a limited dNTP pool [44–46]. However, this reciprocal association was disrupted in cells simultaneously exposed to miR-28 expression and ibrutinib. The reduction in the number of active origins associated with miR-28 treatment was maintained, but the compensatory increase in fork rate was reduced by 35% (Fig. 5C, D). Therefore, miR-28+ibrutinib combination therapy limits DNA replication in DLBCL by simultaneously inhibiting origin activity and the compensatory acceleration of fork progression.

Survival of ABC-DLBCL patients is associated with reduced miR-28+ib signature

To assess whether the specific transcriptional program induced by miR-28+ibrutinib combination therapy is associated with survival differences in DLBCL patients, we ranked 62 ABC-DLBCL patients treated with R-CHOP immunochemotherapy and with 8 years of outcome data [4]. The ranking was based on a singscore analysis [21, 22] of the pretreatment expression of the 114 downregulated genes of the miR-28+ib signature, such that a high score corresponds to higher expression and a low score to downregulated expression (Fig. 6A). miR-28+ib signature scores were not associated with a particular ABC-DLBCL genetic subtype, and there were no significant differences in the proportions of BN2, MCD, and N1 genetic subtypes between patients with scores in the top (high expression) and bottom (low expression) tertiles (Fig. 6B). Correlation with outcome data revealed that patients in the low-expression miR-28+ib signature tertile had higher overall survival than those in the high-expression tertile ($p = 0.005$) (Fig. 6C). We found that miR-28+ibrutinib combination therapy in SUDHL4 cells promoted significant downregulation of 22 genes that are contained within the miR-28+ib signature (Table S5D). We used these 22 genes to calculate a new singscore and to rank the 62 ABC-DLBCL patients. The 22-gene and the 114-gene singscores showed a strong correlation among the patients ($R = 0.69$; Fig. 6D). Further, the new ranking of the patients based on the expression of the subset of 22 genes from the miR-28+ib signature showed also significant differences in survival between the extreme tertiles (Fig. 6E). Thus, we have identified sets of genes specifically downregulated by miR-28+ibrutinib combination therapy as important determinants of ABC-DLBCL survival.

DISCUSSION

Despite the identification of molecular targets for DLBCL, a substantial proportion of these aggressive B cell lymphomas continues to present a major clinical challenge [9]. Here, we explored the therapeutic potential for DLBCL of the tumor suppressor miR-28, both as monotherapy and as combination therapy with ibrutinib. miR-28 expression is reduced in DLBCL and other forms of B-NHL [18, 19, 29, 30], and low miR-28 expression in DLBCL is associated with poor prognosis [47]. Using various ABC-DLBCL and GCB-DLBCL cell lines and PDX phase-II preclinical xenograft models [32], we found that miR-28 inhibits DLBCL growth in vivo. Transcriptome profiling of miR-28–treated DLBCL tumors showed downregulation of genes involved in tumorigenesis. In an earlier study, we reported that miR-28 downregulates B-cell expression of a gene network downstream of the BCR signaling pathway and that miR-28 expression inversely correlates with that of genes downstream of BCR signaling, including NF-κB2, IKKB, and Bcl-2 in ABC-DLBCL [19]. Several of the genes

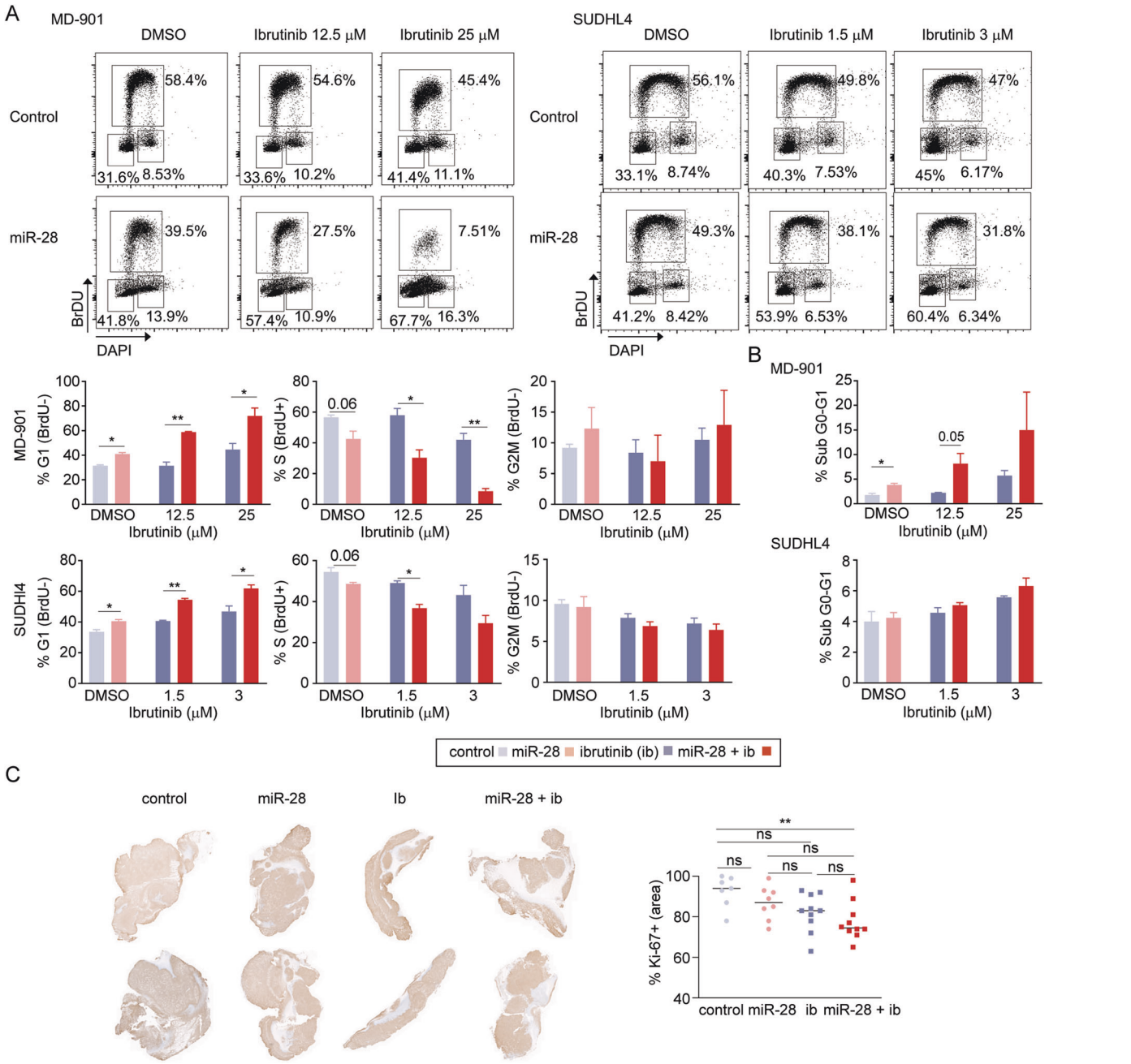

Fig. 4 miR-28 potentiates the ibrutinib anti-tumor effect in DLBCL by promoting cell cycle arrest. A, **B** Cell cycle analysis in doxycycline-induced pTRIPZ-miR-28– or pTRIPZ-scramble–transduced MD-901 and SUDHL4 cells after 20 h of ibrutinib treatment. **A** Representative flow cytometry plots of BrdU incorporation and cell cycle analysis, together with bar plots showing quantitative analysis of 2 independent experiments/cell line. Error bars denote SD. $^{*}P < 0.05$, $^{**}P < 0.01$, unpaired *t* test. **B** Quantification of the Dapi-negative gated sub G0-G1 population. $^{*}P < 0.05$, unpaired *t* test. Error bars denote SD. **C** Proliferation analysis of treated ABC-DLBCL tumors ($n = 7$ control; 8 miR-28; 10 ib; 10 miR-28+ib). Representative images are shown of Ki-67 immunohistochemistry in MD-901 tumors after miR-28 or ibrutinib monotherapy or miR-28+ibrutinib combination therapy. The graph shows quantification of Ki-67+ area $^{**}P < 0.01$, one-way ANOVA. Control (light gray), miR-28 (light pink), ibrutinib (dark gray), miR-28+ibrutinib (dark red).

targeted by miR-28 in B cells, including Bcl-2, NF-κB2 and IRAK1, have been shown to be essential for oncogenic signaling in the ABC and GCB genetic subtypes of DLBCL [48], and our findings are thus in agreement with the anti-tumor effect of miR-28 observed in ABC- and GCB-DLBCL.

Combination therapies are a foundation of cancer treatments because the simultaneous use of two or more agents can target key pathways in a synergistic or additive manner [49]. Ibrutinib monotherapy is initially effective in a high fraction of patients with ABC-DLBCL, but resistance to BTK inhibitors develops rapidly, even in tumors addicted to BCR-dependent NF-*k*B activation, and progression-free survival is therefore very short (2 months) [33, 50]. Ibrutinib combination regimes are currently under exploration [11], and ibrutinib plus R-CHOP chemotherapy has yielded excellent results, but only in young ABC-DLBCL patients with the MCD and N1 genetic subtypes [13]. Therefore, finding new ibrutinib combination therapies is a crucial clinical need for the treatment of DLBCL.

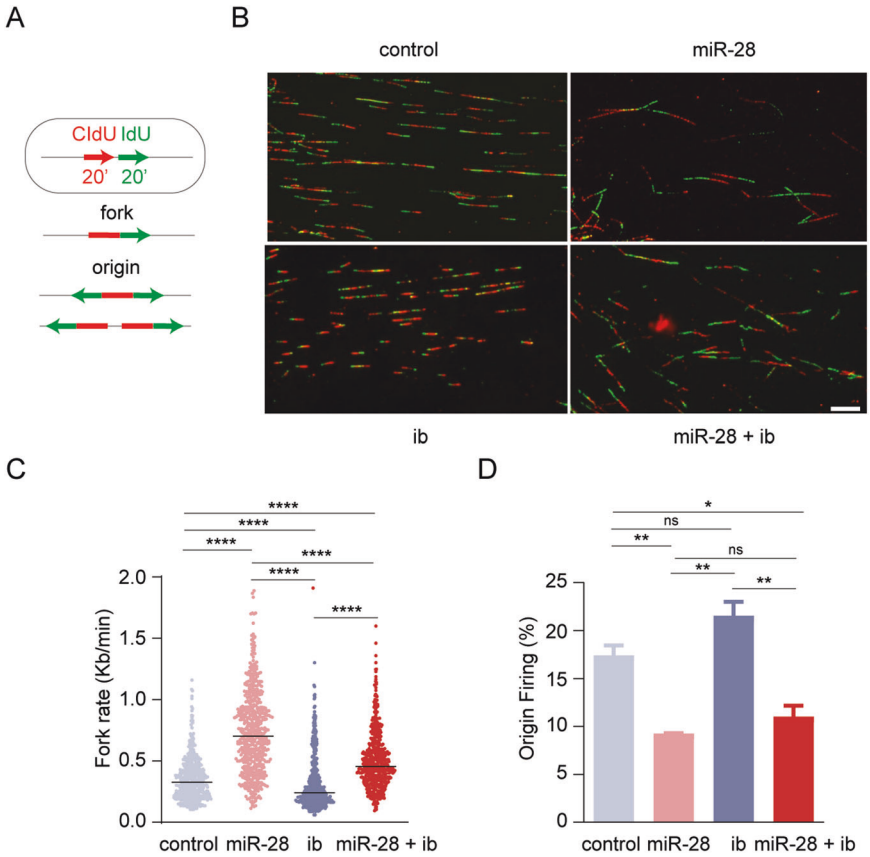

Fig. 5 miR-28+ibrutinib combined treatment impairs DNA replication. A Experimental scheme of a stretched DNA fiber assay performed after 20 h exposure to 12.5 μM ibrutinib of doxycycline-induced pTRIPZ-miR-28 or pTRIPZ-scramble MD-901 cells. Cells were sequentially pulse-labeled with CldU and IdU, and DNA replication patterns (fork rate and origin firing) were measured. **B** Representative images of DNA fibers after miR-28, ibrutinib monotherapy or combined treatment. **C** Dot plot showing the distribution of fork rate under the different conditions. Median values are depicted by horizontal black lines. The plots show data pooled from two replicates ($n > 100$ cells per condition). ****$P < 0.0001$, Kruskal–Wallis test and Dunn's post-test. **D** Origin firing estimated as the percentage of first-label origin structures (mean ± SD; $n = 2$ independent experiments). *$P < 0.05$, **$P < 0.01$, one-way ANOVA.

miRNA-based therapies are especially attractive for cancer and B cell neoplasia because of their potential to simultaneously inhibit multiple targets, which limits the possibility of treatment failure due to tumor evolution through alternative oncogenic pathways and the selection of clones with a treatment-resistant mutation [16, 17]. To our knowledge, this study is the first to assess a miRNA-based combination therapy with ibrutinib. Using in vitro assays and in vivo xenograft models combined with RNA-seq transcriptome profiling, pulsed BrdU incorporation, and DNA fibers assays, we found that miR-28 enhances the anti-tumor effect of ibrutinib by inhibiting a DNA replication and cell cycle transcriptional gene network in DLBCL cells.

The inhibition of this proliferation network specific to miR-28+ibrutinib combination therapy is synergic and not the result of the additive effects induced in gene expression by monotherapy with either agent. This suggests that the molecular actions of miR-28 and ibrutinib intertwine synergistically, likely through the inhibition of parallel pathways involved in DNA replication and cell division in DLBCL cells, such as those emerging from the BCR signaling pathways. We hypothesize that this parallel pathway inhibition would result in the blockage of the compensatory and/or pathway crosstalk activations that can occur after treatment with a single agent. Notably, we found that the transcriptional program induced by miR-28+ibrutinib combination therapy is conserved across different DLBCL cells. Of note, poor DLBCL outcomes have been linked to high expression of proliferation genes and a high Ki-67 proliferation index [51–53]. Likewise, high expression of proliferation genes is considered one of the main oncogenic signatures of DLBCL [4]. Thus, our finding that the set of genes downregulated by miR-28+ibrutinib combination therapy is also downregulated in ABC-DLBCL patients with better survival, strongly supports that this molecular pathway is key to disease outcome. We propose that the miR-28+ib signatures described here can potentially be a valuable new gene expression panel for ABC-DLBCL prognosis and stratification.

Regarding the therapeutic implications, our study provides evidence for the effectiveness of a new miRNA-based ibrutinib combination therapy for DLBCL. The correlation analysis of miR-28+ib signature expression with clinical outcome in an R-CHOP-treated ABC-DLBCL cohort suggests that miR-28+ibrutinib combination therapy would benefit patients with any ABC-DLBCL genetic subtype. Future studies focused on: (i) B-cell lymphoma specific miR-28+ibrutinib delivery approaches, (ii) adjustment of the miR-28 and ibrutinib doses in the combination therapy for the treatment of different DLBCL genetic subtypes, and (iii) analyzing if miR-28+ibrutinib combination therapy reduces the generation of ibrutinib-resistant DLBCL clones, will further increase the translational potential of this work. Interestingly, we have found that miR-28 targets 61 genes essential for ibrutinib-resistant ABC-DLBCL growth [54], including Bcl-2, ORC6, and IRAK1, suggesting that miR-28+ibrutinib combination therapy could reduce the generation of ibrutinib resistance and provide a more durable treatment for DLBCL patients.

In summary, the results of this study provide insights for the development of new diagnostic and therapeutic strategies based on miR-28+ibrutinib combination.

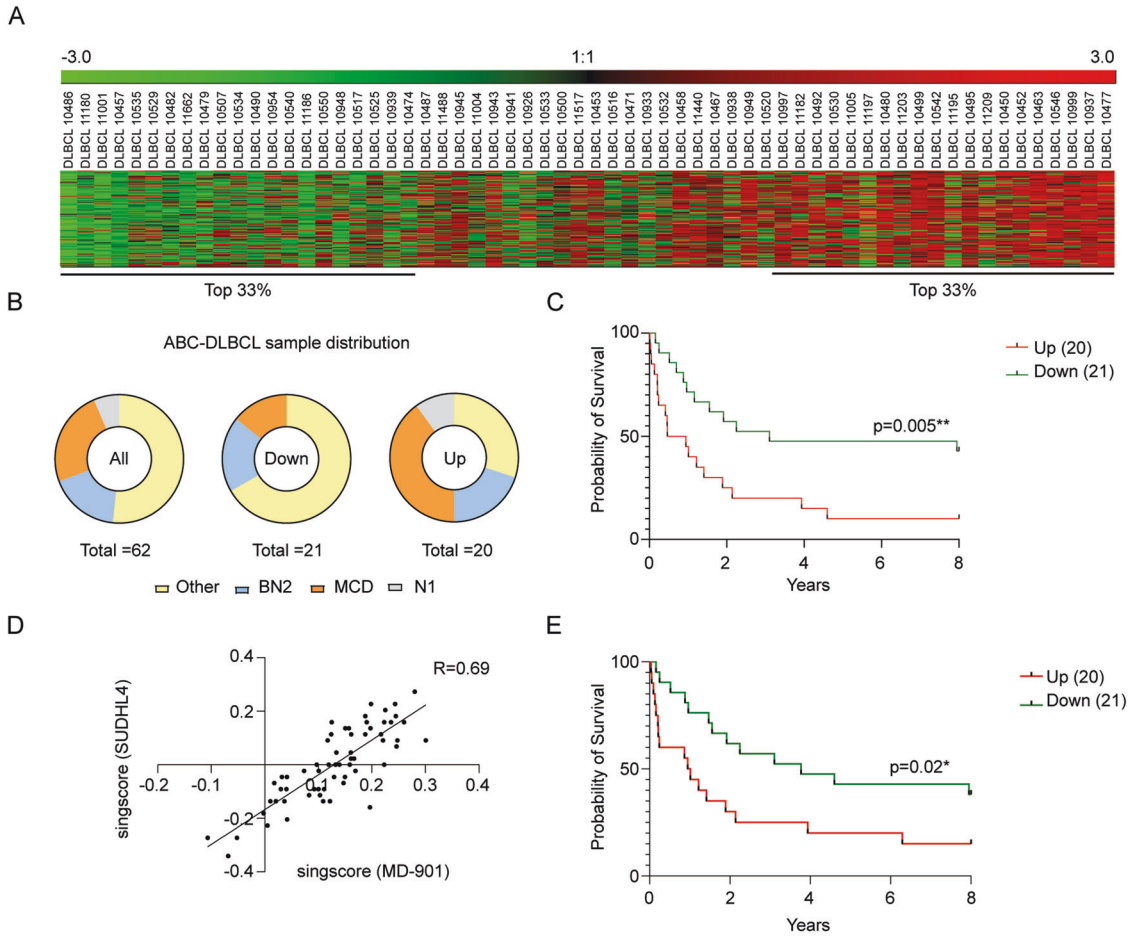

Fig. 6 Downregulation of the miR-28+ib signature is associated with better survival in ABC-DLBCL patients. Survival analysis of ABC-DLBCL patients based on their scored expression of genes in the miR-28+ib signature. **A** Heatmap showing the scored gene expression profiles of 62 ABC-DLBCL patients before R-CHOP treatment for downregulated genes in the miR-28+ib signature, from the lowest expression score (left) to the highest (right). **B** Pie charts showing the distribution of ABC-DLBCL genetic subtypes (Other, BN2, MCD, N1) in all patients (left, $n = 62$), in the 33% of patients with the lowest miR-28+ib signature expression (lowest tertile; middle, $n = 21$), and in the 33% with the highest miR-28+ib signature expression (highest tertile; right, $n = 20$). **C** Kaplan-Meier analysis of ABC-DLBCL patient survival stratified by scored miR-28+ib signature expression: highest expression tertile (Up) in red; lowest expression tertile (Down) in green. $^{**}P < 0.01$. Log-rank (Mantel-Cox) test. **D** Correlation plot of singscore values used to rank ABC-DLBCL patients based on the expression of 114 miR-28+ib signature genes (obtained from MD-901 cells) or a subset of 22 genes from the miR-28+ib signature (obtained from SUDHL4 cells). **E** Kaplan-Meier analysis of ABC-DLBCL patient survival stratified based on the expression of the subset of 22 genes from the miR-28+ib signature which are downregulated after miR-28+ibrutinib combination therapy in SUDHL4 cells. $^{*}P < 0.05$. Log-rank (Mantel-Cox) test.

DATA AVAILABILLITY

The RNA-seq data of the manuscript is available at the GEO Repository (GSE229788).

REFERENCES

1. Susanibar-Adaniya S, Barta SK. 2021 update on diffuse large B cell lymphoma: a review of current data and potential applications on risk stratification and management. Am J Hematol. 2021;96:617–29.
2. Alizadeh AA, Eisen MB, Davis RE, Ma C, Lossos IS, Rosenwald A, et al. Distinct types of diffuse large B-cell lymphoma identified by gene expression profiling. Nature. 2000;403:503–11.
3. Davis RE, Brown KD, Siebenlist U, Staudt LM. Constitutive nuclear factor kappaB activity is required for survival of activated B cell-like diffuse large B cell lymphoma cells. J Exp Med. 2001;194:1861–74.
4. Schmitz R, Wright GW, Huang DW, Johnson CA, Phelan JD, Wang JQ, et al. Genetics and pathogenesis of diffuse large B-cell lymphoma. N. Engl J Med. 2018;378:1396–407.
5. Coiffier B, Lepage E, Briere J, Herbrecht R, Tilly H, Bouabdallah R, et al. CHOP chemotherapy plus rituximab compared with CHOP alone in elderly patients with diffuse large-B-cell lymphoma. N. Engl J Med. 2002;346:235–42.
6. Coiffier B, Thieblemont C, Van Den Neste E, Lepeu G, Plantier I, Castaigne S, et al. Long-term outcome of patients in the LNH-98.5 trial, the first randomized study comparing rituximab-CHOP to standard CHOP chemotherapy in DLBCL patients: a study by the Groupe d'Etudes des Lymphomes de l'Adulte. Blood. 2010;116:2040–5.
7. Lenz G, Wright G, Dave SS, Xiao W, Powell J, Zhao H, et al. Stromal gene signatures in large-B-cell lymphomas. N. Engl J Med. 2008;359:2313–23.
8. Crump M, Neelapu SS, Farooq U, Van Den Neste E, Kuruvilla J, Westin J, et al. Outcomes in refractory diffuse large B-cell lymphoma: results from the international SCHOLAR-1 study. Blood. 2017;130:1800–8.
9. Cheson BD, Nowakowski G, Salles G. Diffuse large B-cell lymphoma: new targets and novel therapies. Blood Cancer J. 2021;11:68.
10. Hou K, Yu Z, Jia Y, Fang H, Shao S, Huang L, et al. Efficacy and safety of ibrutinib in diffuse large B-cell lymphoma: a single-arm meta-analysis. Crit Rev Oncol Hematol. 2020;152:103010.
11. Wen T, Wang J, Shi Y, Qian H, Liu P. Inhibitors targeting Bruton's tyrosine kinase in cancers: drug development advances. Leukemia. 2021;35:312–32.
12. Younes A, Sehn LH, Johnson P, Zinzani PL, Hong X, Zhu J, et al. Randomized phase III trial of Ibrutinib and Rituximab plus cyclophosphamide, doxorubicin, vincristine, and prednisone in non-germinal center B-cell diffuse large B-cell lymphoma. J Clin Oncol. 2019;37:1285–95.

13. Wilson WH, Wright GW, Huang DW, Hodkinson B, Balasubramanian S, Fan Y, et al. Effect of ibrutinib with R-CHOP chemotherapy in genetic subtypes of DLBCL. Cancer Cell. 2021;39:1643–53.e3.
14. Ebert MS, Sharp PA. Roles for microRNAs in conferring robustness to biological processes. Cell. 2012;149:515–24.
15. Fuertes T, Salgado I, de Yebenes VG. microRNA fine-tuning of the germinal center response. Front Immunol. 2021;12:660450.
16. Rupaimoole R, Slack FJ. MicroRNA therapeutics: towards a new era for the management of cancer and other diseases. Nat Rev Drug Discov. 2017;16:203–22.
17. Fuertes T, Ramiro AR, de Yebenes VG. miRNA-based therapies in B cell non-Hodgkin lymphoma. Trends Immunol. 2020;41:932–47.
18. Schneider C, Setty M, Holmes AB, Maute RL, Leslie CS, Mussolin L, et al. MicroRNA 28 controls cell proliferation and is down-regulated in B-cell lymphomas. Proc Natl Acad Sci USA. 2014;111:8185–90.
19. Bartolome-Izquierdo N, de Yebenes VG, Alvarez-Prado AF, Mur SM, Lopez Del Olmo JA, Roa S, et al. miR-28 regulates the germinal center reaction and blocks tumor growth in preclinical models of non-Hodgkin lymphoma. Blood. 2017;129:2408–19.
20. Tompkins VS, Han SS, Olivier A, Syrbu S, Bair T, Button A, et al. Identification of candidate B-lymphoma genes by cross-species gene expression profiling. PLoS One. 2013;8:e76889.
21. Foroutan M, Bhuva DD, Lyu R, Horan K, Cursons J, Davis MJ. Single sample scoring of molecular phenotypes. BMC Bioinforma. 2018;19:404.
22. Bhuva DD, Cursons J, Davis MJ. Stable gene expression for normalisation and single-sample scoring. Nucleic Acids Res. 2020;48:e113.
23. Aparicio T, Guillou E, Coloma J, Montoya G, Mendez J. The human GINS complex associates with Cdc45 and MCM and is essential for DNA replication. Nucleic Acids Res. 2009;37:2087–95.
24. Jackson DA, Pombo A. Replicon clusters are stable units of chromosome structure: evidence that nuclear organization contributes to the efficient activation and propagation of S phase in human cells. J Cell Biol. 1998;140:1285–95.
25. Rodriguez-Acebes S, Mouron S, Mendez J. Uncoupling fork speed and origin activity to identify the primary cause of replicative stress phenotypes. J Biol Chem. 2018;293:12855–61.
26. Laajala TD, Corander J, Saarinen NM, Makela K, Savolainen S, Suominen MI, et al. Improved statistical modeling of tumor growth and treatment effect in preclinical animal studies with highly heterogeneous responses in vivo. Clin Cancer Res. 2012;18:4385–96.
27. Basso K, Sumazin P, Morozov P, Schneider C, Maute RL, Kitagawa Y, et al. Identification of the human mature B cell miRNome. Immunity. 2009;30:744–52.
28. Kuchen S, Resch W, Yamane A, Kuo N, Li Z, Chakraborty T, et al. Regulation of microRNA expression and abundance during lymphopoiesis. Immunity. 2010;32:828–39.
29. Iqbal J, Shen Y, Huang X, Liu Y, Wake L, Liu C, et al. Global microRNA expression profiling uncovers molecular markers for classification and prognosis in aggressive B-cell lymphoma. Blood. 2015;125:1137–45.
30. Li Z, Wong KY, Chan GC, Chim CS. Epigenetic silencing of LPP/miR-28 in multiple myeloma. J Clin Pathol. 2018;71:253–8.
31. Sibley CR, Seow Y, Wood MJ. Novel RNA-based strategies for therapeutic gene silencing. Mol Ther. 2010;18:466–76.
32. Townsend EC, Murakami MA, Christodoulou A, Christie AL, Koster J, DeSouza TA, et al. The public repository of xenografts enables discovery and randomized phase II-like trials in mice. Cancer Cell. 2016;30:183.
33. Wilson WH, Young RM, Schmitz R, Yang Y, Pittaluga S, Wright G, et al. Targeting B cell receptor signaling with ibrutinib in diffuse large B cell lymphoma. Nat Med. 2015;21:922–6.
34. Gambus A, Jones RC, Sanchez-Diaz A, Kanemaki M, van Deursen F, Edmondson RD, et al. GINS maintains association of Cdc45 with MCM in replisome progression complexes at eukaryotic DNA replication forks. Nat Cell Biol. 2006;8:358–66.
35. Pacek M, Tutter AV, Kubota Y, Takisawa H, Walter JC. Localization of MCM2-7, Cdc45, and GINS to the site of DNA unwinding during eukaryotic DNA replication. Mol Cell. 2006;21:581–7.
36. Nagahama Y, Ueno M, Miyamoto S, Morii E, Minami T, Mochizuki N, et al. PSF1, a DNA replication factor expressed widely in stem and progenitor cells, drives tumorigenic and metastatic properties. Cancer Res. 2010;70:1215–24.
37. Nordlund P, Reichard P. Ribonucleotide reductases. Annu Rev Biochem. 2006;75:681–706.
38. Goss KL, Koppenhafer SL, Waters T, Terry WW, Wen KK, Wu M, et al. The translational repressor 4E-BP1 regulates RRM2 levels and functions as a tumor suppressor in Ewing sarcoma tumors. Oncogene. 2021;40:564–77.
39. Nishiyama A, Yamaguchi L, Sharif J, Johmura Y, Kawamura T, Nakanishi K, et al. Uhrf1-dependent H3K23 ubiquitylation couples maintenance DNA methylation and replication. Nature. 2013;502:249–53.
40. Xiang H, Yuan L, Gao X, Alexander PB, Lopez O, Lau C, et al. UHRF1 is required for basal stem cell proliferation in response to airway injury. Cell Discov. 2017;3:17019.
41. Fragkos M, Ganier O, Coulombe P, Mechali M. DNA replication origin activation in space and time. Nat Rev Mol Cell Biol. 2015;16:360–74.
42. Ge XQ, Jackson DA, Blow JJ. Dormant origins licensed by excess Mcm2-7 are required for human cells to survive replicative stress. Genes Dev. 2007;21:3331–41.
43. Ibarra A, Schwob E, Mendez J. Excess MCM proteins protect human cells from replicative stress by licensing backup origins of replication. Proc Natl Acad Sci USA. 2008;105:8956–61.
44. Anglana M, Apiou F, Bensimon A, Debatisse M. Dynamics of DNA replication in mammalian somatic cells: nucleotide pool modulates origin choice and interorigin spacing. Cell. 2003;114:385–94.
45. Zhong Y, Nellimoottil T, Peace JM, Knott SR, Villwock SK, Yee JM, et al. The level of origin firing inversely affects the rate of replication fork progression. J Cell Biol. 2013;201:373–83.
46. Poli J, Tsaponina O, Crabbe L, Keszthelyi A, Pantesco V, Chabes A, et al. dNTP pools determine fork progression and origin usage under replication stress. EMBO J. 2012;31:883–94.
47. Lim EL, Trinh DL, Scott DW, Chu A, Krzywinski M, Zhao Y, et al. Comprehensive miRNA sequence analysis reveals survival differences in diffuse large B-cell lymphoma patients. Genome Biol. 2015;16:18.
48. Phelan JD, Young RM, Webster DE, Roulland S, Wright GW, Kasbekar M, et al. A multiprotein supercomplex controlling oncogenic signalling in lymphoma. Nature. 2018;560:387–91.
49. Bayat Mokhtari R, Homayouni TS, Baluch N, Morgatskaya E, Kumar S, Das B, et al. Combination therapy in combating cancer. Oncotarget. 2017;8:38022–43.
50. Xue C, Wang X, Zhang L, Qu Q, Zhang Q, Jiang Y. Ibrutinib in B-cell lymphoma: single fighter might be enough? Cancer Cell Int. 2020;20:467.
51. Rosenwald A, Wright G, Chan WC, Connors JM, Campo E, Fisher RI, et al. The use of molecular profiling to predict survival after chemotherapy for diffuse large-B-cell lymphoma. N. Engl J Med. 2002;346:1937–47.
52. Li ZM, Huang JJ, Xia Y, Zhu YJ, Zhao W, Wei WX, et al. High Ki-67 expression in diffuse large B-cell lymphoma patients with non-germinal center subtype indicates limited survival benefit from R-CHOP therapy. Eur J Haematol. 2012;88:510–7.
53. Miller TP, Grogan TM, Dahlberg S, Spier CM, Braziel RM, Banks PM, et al. Prognostic significance of the Ki-67-associated proliferative antigen in aggressive non-Hodgkin's lymphomas: a prospective Southwest Oncology Group trial. Blood. 1994;83:1460–6.
54. Shaffer AL 3rd, Phelan JD, Wang JQ, Huang D, Wright GW, Kasbekar M, et al. Overcoming acquired epigenetic resistance to BTK inhibitors. Blood Cancer Discov. 2021;2:630–47.

ACKNOWLEDGEMENTS

We thank Simon Bartlett for English editing. T.F.N. and P.U.-C. were supported by PhD fellowships from the Spanish Ministerio de Ciencia, Innovacion y Universidades (BES-2017-079759 and BES-2017-081887, respectively), CG-E by a PhD fellowship awarded by La Caixa España 2017, AS-N by a FPI Severo Ochoa fellow (PRE2018-083475), E.A.C. by funding from the Comunidad de Madrid (CT4/21/PEJ-2020-AI/BMD-18112), A.R.R. by CNIC funding and V.G.Y. by the Universidad Complutense de Madrid. This work was funded by Spanish Ministerio de Ciencia e Innovación grants PID2019-107551RB-I00/AEI/10.13039/501100011033 to V.G.Y., PID2019-106773RB-I00/ AEI / 10.13039/501100011033 to A.R.R. and PID2019-106707RB-100/AEI/10.13039/50110001103 v to J.M., co-sponsored by EU ERDF funds. The CNIC is supported by the Instituto de Salud Carlos III (ISCIII), the Ministerio de Ciencia e Innovación (MCIN) and the Pro CNIC Foundation), and is a Severo Ochoa Center of Excellence (grant CEX2020-001041-S funded by MICIN/AEI/10.13039/501100011033). The authors wish to thank the donors, and the Hospital Universitario Puerta de Hierro Majadahonda (HUPHM)/ Instituto de Investigación Sanitaria Puerta de Hierro-Segovia de Arana (IDIPHISA) Biobank (Carlos III Health Institute Biobanks and Biomodels Platform) and the Public Repository of Xenografts from the Dana Farber Cancer Institute for the human specimens used in this study.

AUTHOR CONTRIBUTIONS

T.F., E.A.C. and P.U-C performed experiments. A.S.N. and C.G.E. performed computational analysis. T.F., E.A.C, P.U, A.M. and V.G.Y. analyzed and interpreted data. T.F. prepared figures. J.M. contributed to the conception of the experimental design. V.G.Y and A.R.R. conceived the overall strategy. V.G.Y, T.F. and A.R.R. wrote the manuscript. All authors revised and contributed to the final manuscript.

COMPETING INTERESTS

The authors declare no competing interests.

ADDITIONAL INFORMATION

Supplementary information The online version contains supplementary material available at https://doi.org/10.1038/s41419-023-06178-0.

Correspondence and requests for materials should be addressed to Almudena R. Ramiro or Virginia G. de Yébenes.

Reprints and permission information is available at http://www.nature.com/reprints

Publisher's note Springer Nature remains neutral with regard to jurisdictional claims in published maps and institutional affiliations.